16A.6 **GUST FRONT VS. NON-GUST FRONT THUNDERSTORMS: APPLICATION OF THE MULTI-RESPONSE PERMUTATION PROCEDURE (MRPP) TO ASSESS RADAR STORM CHARACTERISTICS AND ENVIRONMENTAL CONDITIONS**

Theresa A. Aguilar[+]*
Tammy M. Weckwerth[^]
Donna V. Kliche[+]
Rita D. Roberts[^]
Paul L. Smith[+]
South Dakota School of Mines & Technology, Rapid City, SD[+]
National Center for Atmospheric Research, Boulder, CO[^]

1. INTRODUCTION

The purpose of this paper is to highlight the use of a non-classical, rigorous statistical technique, called the Multi-Response Permutation Procedure (MRPP), to differentiate gust front (GF) and non-gust front (NGF) thunderstorms observed during the 2002 International H_2O Project (IHOP_2002). Given that this mesoscale feature has a considerable influence on thunderstorm development and behavior with the potential to initiate secondary convection, it is essential, particularly for short-term forecasting, to know which storms will produce a gust front. However, this research did not focus on gust front forecasting, rather, the objective was to identify significant variables that distinguished GF/NGF storms, in terms of storm radar characteristics and environmental conditions, using a probability approach (though the preliminary results could be used as predictors in gust front development).

2. MRPP

MRPP is a statistical procedure which tests the null hypothesis that two or more groups exhibit no differences (McCune and Grace 2002). More specifically, MRPP is based on absolute differences, is resistant to outliers, and does not require parametric assumptions of normality, as is often the case with classical analysis (Biondini et al. 1988). The only assumption with MRPP is that the units of the groups in question are interchangeable; if not, rank values are used instead. Mielke et. al. (1981) demonstrated the application of MRPP by using a simple dataset for two groups (A and B) of interest with measurements of two variables (X_1 and X_2) corresponding to 3 members of A and 4 members of B (Fig. 1). In the context of this research, groups A and B could be considered GF and NGF storms, respectively, where the members correspond to the number of case studies in each group, and the variables of interest (X_1, $X_{2...}$) are atmospheric measurements (i.e., convective available potential energy, convective inhibition, etc.).

*Corresponding author: Theresa A. Aguilar, email: theresa.gail.aguilar@gmail.com

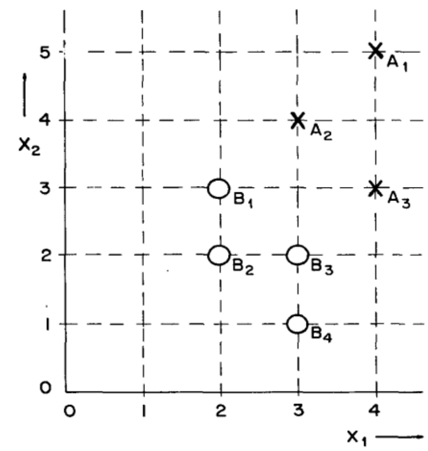

Figure 1. Scatter plot comparing two groups (A and B) with a total of seven measurements for two variables (X_1 and X_2). Source: Mielke et al. (1981).

Based on visual inspection of Fig. 1, there appears to be clear separation between groups A and B, or clustering of similar groups. To objectively assess this separation/clustering, Mielke et al. (1981) first calculated the Euclidean distances between points of a similar group (i.e., A_1A_2, A_1A_3,…; B_1B_2, B_1B_3,…) as well as a different group (A_1B_1, A_1B_2,…). The average Euclidean distance of a similar group was then calculated for group A (1.609) and group B (1.3441), which were used to compute the weighted mean (1.4578). The weighted mean provided a measure that described the separation between the points of group A and those of group B.

The remaining step for Mielke et al. (1981) was to determine if the weighted mean, for this particular situation, was unusual with respect to all other possible outcomes based on the same size structure that could be made with other allocations of the seven data points to the two groups. Mielke et al. (1981) determined there were 35 possible outcomes (weighted means), shown in Table 1 in ascending order. The weighted mean for group A and B (1.4578) was ranked 1 out of 35 with a calculated p-value (chance of an equal or smaller weighted mean) of 0.0286, which is considered statistically significant (i.e. less than 0.05 or 0.1). Therefore, for this case, the null hypothesis was rejected.

Table 1. List of all 35 possible weighted mean distances in ascending order. Source: Mielke et al. (1981).

Rank	Value	Rank	Value
1	1.4578	19	2.1381
2	1.5421	20	2.1480
3	1.6939	21	2.1591
4	1.7505	22	2.1646
5	1.8389	23	2.1709
6	1.8547	24	2.1740
7	1.8935	25	2.1769
8	1.9898	26	2.1891
9	1.9915	27	2.1939
10	1.9988	28	2.2025
11	2.0060	29	2.2169
12	2.0157	30	2.2258
13	2.0176	31	2.2280
14	2.0522	32	2.2470
15	2.0575	33	2.2518
16	2.0829	34	2.2812
17	2.0944	35	2.2935
18	2.1158		

To summarize, MRPP examines the distances of data points within each group and compares them to the distances of the data points between the groups. It stands to reason that if a group is truly similar, then the within-group distances should be smaller compared to the between-group distances. By using probability values, MRPP provides a quantitative approach to test the null hypothesis. More specifically, MRPP can also be used to determine which variables of interest have the most effect in reducing the p-value..

In this research, the null hypothesis was that GF and NGF storms exhibit no differences in terms of storm radar characteristics and environmental conditions. While the null hypothesis was simple to test using MRPP, the primary challenges involved selecting the variables of interest for storm & environmental assessments as well as how to structure that data for MRPP (especially for storm characteristics). The next few sections will discuss the data source for this research, the atmospheric variables selected for evaluation, and the data setup for the MRPP technique.

3. DATA SOURCE

The GF and NGF thunderstorms analyzed in this study were observed during the IHOP_2002 field campaign, which was conducted over the Southern Great Plains (Fig. 2) for approximately six weeks, May through June in 2002. More specifically, within the IHOP domain and among the extensive instrumentation available, this research focused exclusively on the location and coverage by the National Center for Atmospheric Research (NCAR) S-band dual-polarization Doppler radar, S-Pol. S-Pol was situated in the panhandle of Oklahoma with coverage extending over southwest Kansas, the extreme southeast portion of Colorado, and the panhandle of Texas. S-Pol provided measurements every 5 to 10 min for traditional and polarimetric fields, which assisted in the analysis of storm characteristics.

S-Pol's radar reflectivity and Doppler velocity data were used to identify and verify GF/NGF thunderstorms during IHOP_2002. Initially, storms that either developed within or propagated through S-Pol's domain were documented and, with the use of surface analysis maps, organized based on the synoptic setup. As a result, there were originally 12 synoptic events of interest, each event acting as the common forcing mechanism for a given number of thunderstorms. However, when the initiation location (within S-Pol coverage) and storm type criteria (single & multi-cell storms only) became established, the number of synoptic events was reduced. The corresponding storms for each event were then identified as either GF or NGF depending on whether or not a divergence signature was present in the lowest radar elevation angle of the velocity field. As a result, 14 thunderstorms, associated with 6 synoptic events, were selected for this study. The breakdown of each event, number of associated storms, and number of GF/NGF storms are shown in Table 2. Of the 14 thunderstorms, 9 were identified as GF and 5 as NGF storms (Fig. 3).

It should be noted that from the 6 synoptic events, the most prevalent synoptic setup for GF storms involved the stationary front and in some cases its interaction with the dryline. Other observed synoptic-scale setups involved the cold front and trough line features, while in some cases there was an absence of large-scale forcing. For the NGF storms, the most prevalent synoptic setup was actually the lack of any large-scale forcing source. However, this region is often influenced by strong south/southeasterly surface winds as well as the low level jet phenomena. In the absence of large-scale forcing, these features can make it difficult for a thunderstorm outflow to penetrate to the surface and be detected on radar.

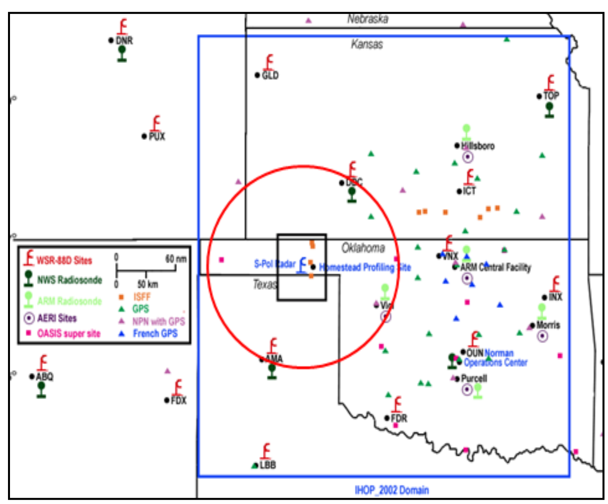

Figure 2. Overview map of the IHOP_2002 domain (blue box) and instrumentation coverage. The embedded black box shows the location of S-Pol and the overlaid red circle is the approximate radar coverage. Source: Weckwerth et al. (2004).

Table 2. List of synoptic events and associated thunderstorms identified during IHOP_2002. From this list, information about the event number, date, number of storms, and number of GF/NGF storms are provided.

Event No.	Date	Total No. of Storms	No. of GF/NGF Storms
1	05/15 – 05/17	---	---
2	05/20	---	---
3	05/24	4	3 / 1
4	05/26	1	1 / 0
5	05/29 – 05/30	---	---
6	06/02 – 06/05	---	---
7	06/10 , 06/11	3	2 / 1
8	06/12 – 06/13	1	1 / 0
9	06/14	---	---
10	06/15	4	1 / 3
11	06/17	1	1 / 0
12	06/20	---	---

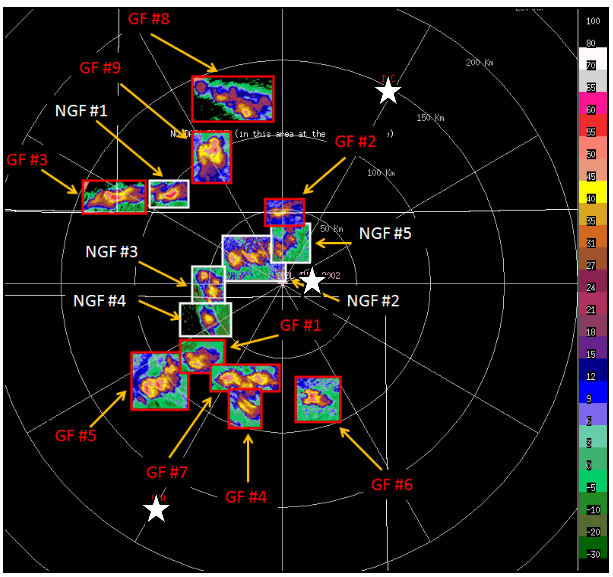

Figure 3. Radar composite of selected individual storms with respect to S-Pol. Red and white colors indicate GF and NGF storms, respectively. The white stars correspond to the three sounding locations: AMA, DDC, and ISS.

To assess the environmental conditions associated with these selected cases, thermodynamic skew-t diagrams, obtained from radiosondes launched at different sites within S-Pol's domain, were utilized. The soundings were acquired from three particular locations: NCAR's Integrated Sounding System (ISS) site (just east of S-Pol's location) and the National Weather Service sites in Amarillo, TX (AMA) and Dodge City, KS (DDC), as shown in Fig. 3. However, it should be noted that the soundings were launched based on IHOP_2002's objective (mission) of the day, which impacted sounding availability for this study. In addition, a moisture bias was discovered between the radiosondes launched by DDC and the ones launched by the AMA and ISS sites. The moisture biases were later corrected by NCAR's Earth Observing Laboratory Data Management Group and used in this research.

As a result of limitations and concerns associated with the soundings (location, availability, and timing), a "first-cut" approach was implemented, meaning that the environmental conditions analyzed were derived for the time the soundings were taken. The time between when the storms initiated and when the soundings were taken varied from an hour to approximately six hours. Since three fixed sites were used, care was taken in selecting soundings that were representative of the pre-storm environments. Using analyzed surface maps and radar reflectivity, encompassing the time from when the soundings were launched to when (and where) storms initiated, assisted with the site selection. This was to ensure that no boundary passages occurred (e.g., cold front, gust front) between the sounding launch time and the time of storm initiation. To analyze the IHOP_2002 soundings, NCAR's System for User-editing and Display of Soundings (SUDS) program was employed. The next section will discuss the specific variables selected to assess storm characteristics and environmental conditions.

4. Data Selection & Setup

Since gust fronts are a product of collective downdrafts in a thunderstorm and are initiated/enhanced by different methods, such as precipitation drag and melting/evaporation processes, it was important to consider the microphysics of hydrometeors. Several modeling studies have shown the impact of hydrometeor size and type on downdraft formation and intensity (i.e., Srivastava 1987, 1988; van den Heever and Cotton 2004). For instance, Hookings (1965) found that vigorous downdrafts were produced with smaller drop sizes, greater liquid-water content, and lower initial humidity at the downdraft origin. Rasmussen et al. (1984) observed that the melting of small hail and frozen drops was very effective in cooling the air around the falling precipitation. In addition, the surface roughness and shape irregularities of the frozen hydrometeors contributed to a significant decrease in melting time, which provided a stronger region of cooler, denser air.

More recently, van den Heever and Cotton (2004) tested the sensitivity of simulated supercell thunderstorms by varying the mean hail size distributions and found a strong influence on the melting and evaporation rates. With small hail, greater rates of melting and evaporation produced stronger downdrafts which resulted in a "runaway" gust front causing the supercell thunderstorm to weaken and vice versa for larger hail. Other sensitivity studies have documented similar impacts on simulated convective storms (e.g., Johnson et al. 1983; Schlesinger 1999; Gilmore et al. 2004).

Given the importance of hydrometeors on thunderstorm gust fronts, variables related to its microphysical properties (i.e., particle shape, orientation, phase, bulk density, etc.) were examined for the storm characteristics. Specifically, radar measurements of **Reflectivity (Z)**, **Differential Reflectivity (Z_{dr})**, **Specific Differential Phase (K_{dp})**, **Linear Depolarization Ratio (LDR)**, and **Copolar Correlation Coefficient (Rho_{hv})** were used. **Storm Area** and the **Particle Identification (PID)** field were also incorporated. In total, there were 7 variables analyzed for storm characteristics.

As for environmental conditions, gust front characteristics are dictated not only by the behavior of the parent thunderstorm but also by the flow and stratification of the environment (Simpson 1969; Goff 1976; Wakimoto 1982; Droegemeier and Wilhelmson 1987). For instance, Goff (1976) analyzed the characteristics of 20 thunderstorm outflows using a 461 m tower and found that if the environment was characterized by a strong surface inversion, the outflow would either have difficulty dislodging the denser air or overriding the inversion. If the inversion was elevated, then there was no well-defined gust front at low-levels.

In another study, McCaul and Cohen (2002) used a cloud model to explore the sensitivity of thunderstorms to mixed and moist layer depths, which were approximated by the heights of the lifted condensation level (LCL) and level of free convection (LFC). In addition, the study used a moderately sheared curved hodograph, which was ideal for examining the transition between supercell/multicell behavior and gust front development. The study observed that under a starved convective available potential energy (CAPE = 800 J kg^{-1}) environment, the simulated storms became large, intense supercell thunderstorms when the height of the LCL = LFC was within 1.5 to 2.5 km above ground. And in a shear starved environment with sufficient CAPE (CAPE = 2000 J kg^{-1}), there was a tendency toward mutlicell development and gust front dominance when the height of the LCL = LFC was higher.

Therefore, for this research study, basic variables that characterized moisture, instability and shear were examined. The following 18 environmental variables were selected:

- **Surface potential temperature (PT) & virtual potential temperature (VPT),**
- **Surface mixing ratio (MR, 50 mb avg.),**
- **400 mb temperature (T), potential temperature (PT), virtual temperature (VT), virtual potential temperature (VPT),**
- **700 mb mixing ratio (MR, 50 mb avg.),**
- **Melting level (ML),**
- **LCL,**
- **Modified lifted index (MLI),**
- **LFC,**
- **CAPE & convective inhibition (CIN),**
- **Positive area below LFC & negative area above LFC,**
- **0-6 km shear, and**
- **Bulk Richardson number.**

Once the variables of interest were identified for storm characteristics and environmental conditions, the next task involved extracting the data. While the environmental conditions were straightforward in terms of applying MRPP, there were more steps involved with extracting the radar data for storm characteristics, which are discussed in the next section.

4.1 Radar Storm Characteristics

The challenge with storm characteristics was analyzing the case studies concisely, since thunderstorms tend to vary-spatially, temporally, and with height. In past studies, particularly Knight et al. (2008) and Wilson et al. (2011), a technique was implemented that analyzed the area of a thunderstorm cell for each radar-scanned elevation angle and time frame available. This allowed for time-height profiles to be created for different radar fields. This research utilized the same method to create time-height profiles for the selected polarimetric radar fields.

A polygon-drawing program, developed for Wilson et al. (2011), was also employed in this research. The program allows a user to draw polygons around a storm, calculating basic statistics for each radar product. More specifically, for each polygon drawn, "average" values for *A*Z, AZ_{dr}, AK_{dp}, $ARho_{hv}$, and *A*LDR can be computed. As explained in Wilson et al. (2011), the *A* denotes the single average numbers calculated over the area of the cell. That is, for each radar field, the values for all range gates (or pixels) within the polygon area are summed and then averaged. For the time scale, each *A*-value was plotted at the registered time of the start of an elevation sweep. For height, each *A*-value was plotted at the mid-beam height that corresponded to the range of a polygon's center. Figure 4 shows an example of the process for creating an *A*Z time-height profile for one thunderstorm event. To assure the quality of the radar values used in calculating the averages, thresholds were applied to each radar field (see Appendix A).

In order to determine a mutual region to analyze for both GF and NGF storms, the *A*Z time-height profiles were contoured by hand. When the approximate low-level divergence times were marked for the GF storms, it was noted that they all occurred during the strongest reflectivity core. The decision was then made to also concentrate on the strongest reflectivity core region and similar time frame for NGF storms. A 5-by-5 data extraction grid was placed on the mean time-height profiles for each storm characteristic. For the GF storms, the placement of the 5-by-5 grid was based on the following: a) the approximate low-level divergence time as determined in the velocity field, b) the four time steps prior to the divergence time (~10 min. apart), and c) the lowest 5 elevation angles available.

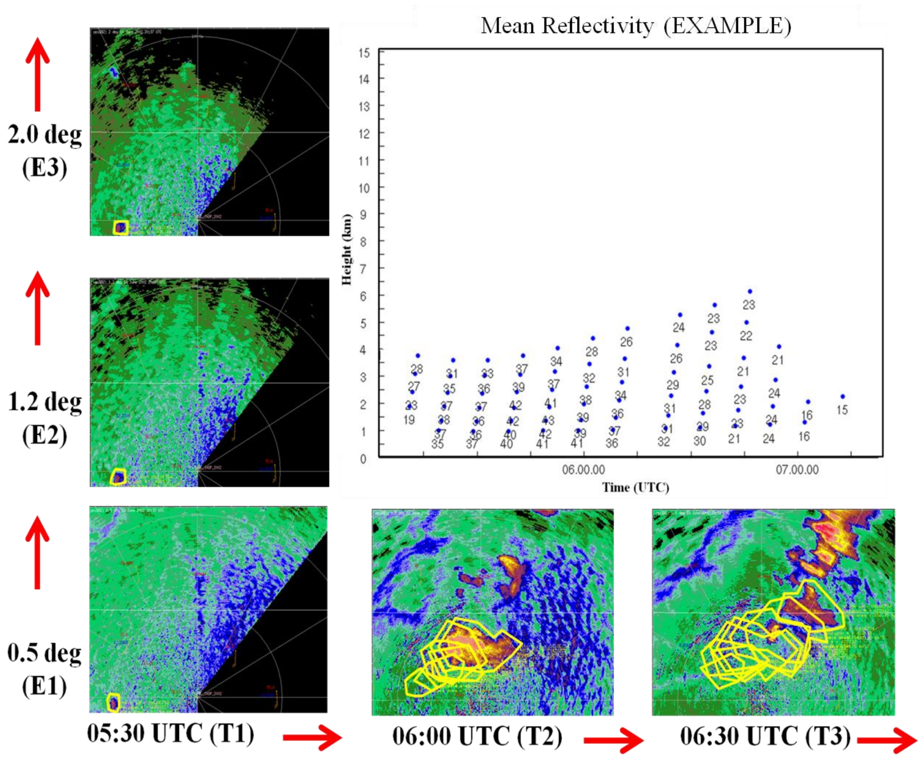

Figure 4. Procedure for creating time-height plots. A polygon is drawn around the storm using the radar reflectivity for each elevation angle (E) and time step (T) available. A mean reflectivity value is calculated for each polygon and used to create the time-height plot (blue dots). Mean values for the other polarimetric fields (not shown) are automatically calculated.

For NGF storms, the only difference was that the placement of the 5-by-5 grid was based on the approximate time the strongest reflectivity core began to decay. An example of the focus area associated with a GF and NGF storm is illustrated in Figures 5A-B.

It is important to note that the radar elevation angle was used instead of height for organization. Since there was uncertainty in the application and where the extraction approach would take this research, it was simpler to keep the data organized by elevation angle. The primary radar elevation angles were 0, 0.5, 1.2, 2, and 3 deg. Even then, there were issues due to inconsistencies in the availability of radar measurements for the different elevation angles. Therefore, the elevation angles were simply labeled E1-E5; a similar notation was used for time, time steps T1-T5 (Fig. 6). Moreover, since there was variability in the distances of the storms from the radar, the organization of the data meant the application of MRPP had to be adjusted to account for range dependency.

In order to determine which storm characteristics and elevation angles/heights differentiated GF and NGF storms, MRPP was applied to each time step. As a result, there were 30 radar variables: 6 storm characteristics at 5 elevation angles for **1** time step (PID was analyzed separately). Rank values for storm characteristics were used instead of actual values since it was necessary for the computation of Euclidean distances in MRPP (Table 3).

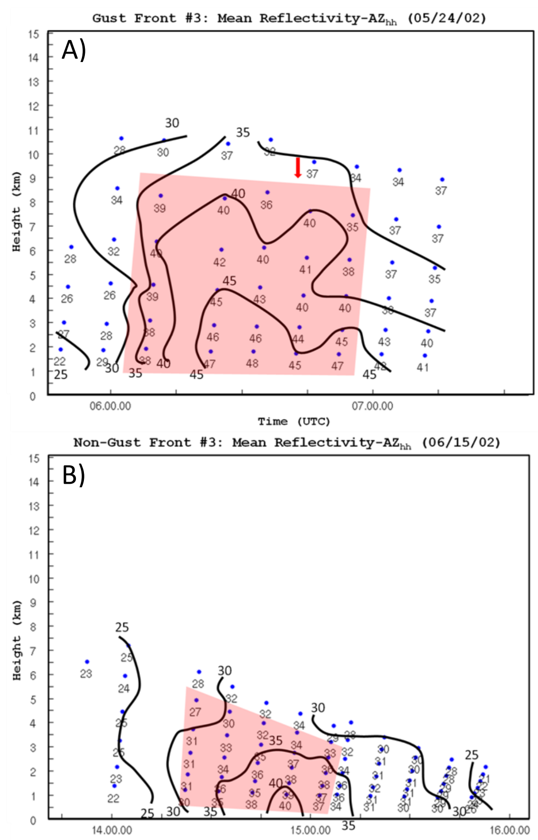

Figure 5. Time-height plots of contoured mean reflectivity for A) GF storm and B) NGF storm. Shaded red box highlights the radar data extracted from each storm and the red arrow marks the ~divergence time for the GF storm.

Table 3. Example data organization for a few storm characteristics. This example was based on time step 1 with elevation angle 1 data for GF storms and elevation angle 2 data for NGF storms. Top table shows actual mean values observed while the bottom table is the corresponding ranks of the GF and NGF storms for each storm characteristic.

Storm ID	AZ (dBZ)	AZ_{dr} (dB)	AK_{dp} (deg km^{-1})
GF #1	28.998	2.57996	-0.117455
GF#2	37.4211	2.83744	0.137316
GF #3	37.741	0.928443	-0.123548
GF #4	26.7783	1.76179	0.359354
GF #5	33.3922	2.23639	0.0264207
GF #6	31.6475	3.16983	0.163385
GF #7	47.9399	3.12009	0.538205
GF #8	30.626	2.05453	-0.0948683
GF #9	28.8597	3.11975	-0.296961
NGF #1	36.0101	1.68178	-0.0188709
NGF #2	42.8733	2.99361	0.143399
NGF #3	29.9658	2.53948	0.39
NGF #4	24.8975	2.31465	0.138749
NGF #5	28.342	2.76132	-0.046264

Storm ID	AZ (rank)	AZ_{dr} (rank)	AK_{dp} (rank)
GF #1	5	8	3
GF#2	11	10	8
GF #3	12	1	2
GF #4	2	3	12
GF #5	9	5	7
GF #6	8	14	11
GF #7	14	13	14
GF #8	7	4	4
GF #9	4	12	1
NGF #1	10	2	6
NGF #2	13	11	10
NGF #3	6	7	13
NGF #4	1	6	9
NGF #5	3	9	5

In each time step, a baseline MRPP p-value was first established for comparison but it was usually so high that it failed to reject the null hypothesis. Each storm characteristic was then removed one at a time and a new p-value was calculated. If the new p-value became higher (worse) than the baseline p-value, it meant that the variable removed was actually significant. A more formal approach involved taking the difference between the baseline p-value and each newly generated p-value to produce a delta p-value (baseline minus new p-value). If the delta p-value was negative, then the associated characteristic was identified as significant. Table 4 shows the MRPP results for time step 1. In this case, the significant storm characteristic was *A*LDR.

The same process was conducted with the elevation angles, where all the storm characteristics for a particular elevation angle were removed and a new p-value calculated. Table 4 shows that for time step 1, the heights corresponding to elevation angles 1-3 and 4-5 were found significant. MRPP was then applied once more but only on the storm characteristics and elevation angles that were found significant. The combinations that arrived at a p-value ≤ 0.1 were considered to be of further interest. A p-value of 0.015 was calculated for *A*LDR at elevation angles 1-3 and 4-5.

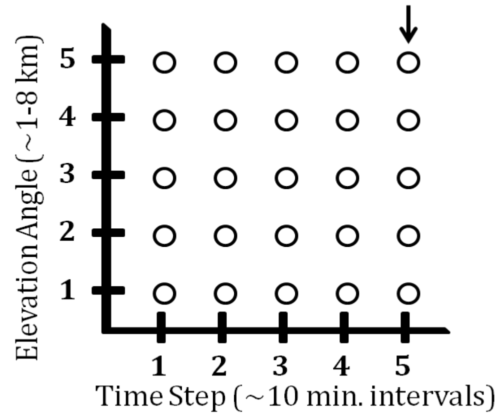

Figure 6. Schematic of the data organization for storm characteristics. Each circle represents the seven variables of interest at that time step and elevation angle. Arrow represents the approximate divergence or decay time for GF and NGF storms, respectively.

As mentioned previously, there was a range dependency as a result of data organization by elevation angle. To address this issue, there was overlap when elevation angles were removed. For example, for 1 time step, all storm characteristics at elevation angle 1 and 2 were removed and a p-value was calculated, then the next removal was elevation angle 2 and 3, and so forth (hence, E1-E2).

The lowest elevation angle of the two was always associated with the GF storms, since these storms were the farthest from the radar relative to the NGF storms, while the highest elevation angle of the two was reserved for NGF storms. This was done to ensure that roughly the same region, in terms of height, was considered in the analysis. The results are discussed in the next section.

Table 4. MRPP results for time step 1, roughly 40 min prior to divergence time/decay time. The (*) indicates the baseline p-value used for comparison. Storm characteristics and elevation angles identified as significant were based on negative delta p-values (bold).

Storm Characteristic	P-Value	Delta P-Value
All*	0.172*	---
No AZ	0.094	0.078
No AZ_{dr}	0.145	0.027
No AK_{dp}	0.152	0.020
No $ARho_{hv}$	0.137	0.035
No ALDR	**0.360**	**-0.188**
No Storm Area	0.154	0.018
Elevation Angle	**P-Value**	**Delta P-Value**
No E1-E2	**0.197**	**-0.025**
No E2-E3	**0.186**	**-0.014**
No E3-E4	0.162	0.010
No E4-E5	**0.177**	**-0.005**

4.1.1 MRPP Results

The process previously discussed allowed this study to determine not only which radar storm characteristics differentiated GF and NGF storms but more specifically where and when they were significant. The final MRPP results for storm characteristics are shown in Figure 7. For each time step, p-values less than 0.1 were observed for three specific average radar fields: AZ_{dr}, $ARho_{hv}$, and *A*LDR. The location of consistent significance was observed primarily between radar elevation angles 2 and 4, which corresponded to heights approximately 1 to 6 km above ground level (AGL). Surprisingly, there was good continuity between time steps for *A*LDR.

Further inspection, particularly with elevation angles 2 and 3, indicated a region of interest for mean LDR roughly 1 to 4 km AGL, where 4 and 2.5 km were considered the average melting height and LCL, respectively. Figure 8A-E shows the progression of the mean LDR with time for GF and NGF storms. For instance, in time step 1 (Fig. 8A) which was ~40 min. prior to the divergence/decay time, there was separation/clustering around a mean LDR value of -25 dB. The majority of GF storms had higher values ≥ -25 dB relative to NGF storms, which suggested the presence of mixed-phase, irregular-shaped precipitation. This ≥ -25 dB observation for mean LDR remained fairly consistent for time step 2 (~30 min prior to), time step 3 (~20 min prior to), time step 4 (~10 min prior to), and time step 5 (~0 min prior to) as show in Figure 8B-E.

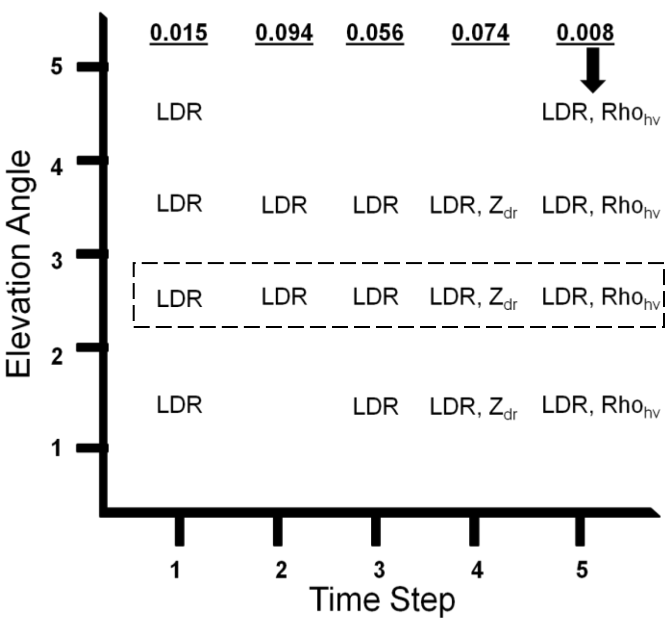

Figure 7. Compilation of significant storm characteristics based on MRPP results. Underlined numbers are p-value results for each time step (~10 min. each) leading up to the divergence/decay time for GF and NGF storms, respectively (black arrow). LDR is dominant, particularly at elevation angles 2-4. Dashed line highlights the selected elevation angles and time frame analyzed further for LDR.

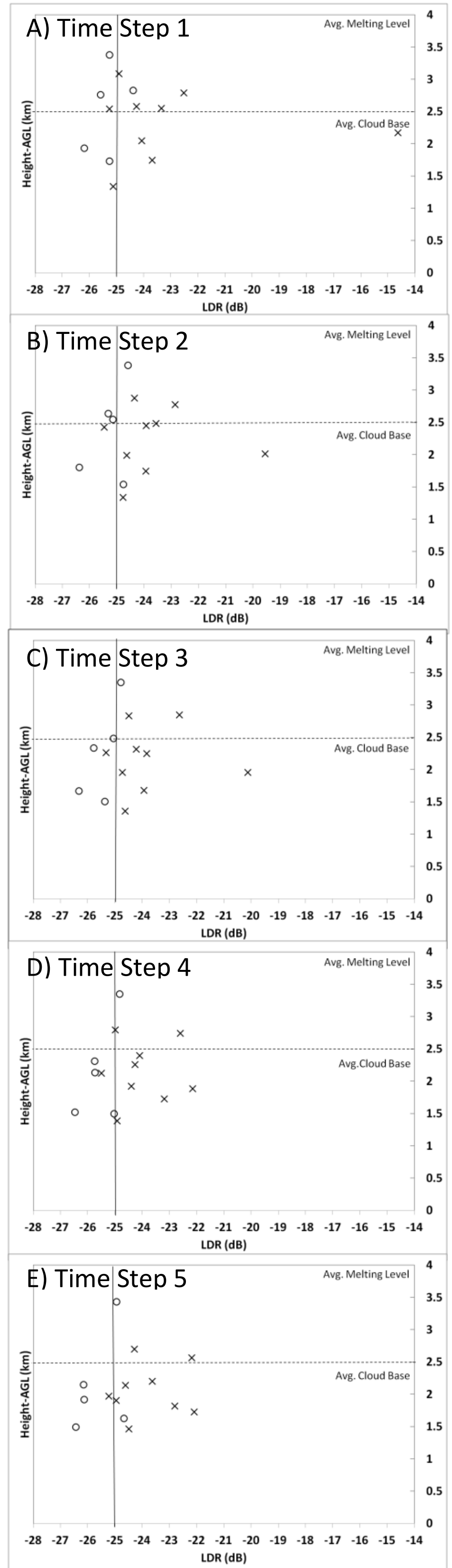

Figure 8. Mean LDR for GF (X's) and NGF (O's) storms at A) time step 1, B) time step 2, C) time step 3, D) time step 4, and E) time step 5. Vertical line marks the -25 dB threshold. The average melting and cloud base heights are also identified.

The examination of the PID field was slightly different compared to the other polarimetric variables. S-Pol provided 14 true hydrometeor categories (i.e., hail, light rain, graupel, etc.) and 3 additional categories reserved for insects, second-trip echo, and clutter (Fig. 9). Since values were categorical, the mode instead of the mean was used in creating the time-height profiles for the PID field and in extraction process. More specifically, the dominant (and even second dominant) hydrometeor type, based on percentages, was considered.

As with mean LDR, similar time series were constructed using the dominant (mode) PID for the same depth (1-4 km AGL) and are shown in Fig. 10A-E. The mode PID had two primary categories present in each time step: light rain and graupel/rain; in some instances, moderate rain and graupel/small hail were also present. There was even more variability in PID categories between GF and NGF storms for the second dominant PID (not shown).

Although the two hydrometeor types associated with the mode PID did not necessarily differentiate GF and NGF storms, the transition from light rain to graupel/rain was observed more so in the majority of GF storms relative to NGF storms. This transition is shown well in Fig. 10A-E, particularly by time step 4 (Fig. 10D). In addition, when the mean LDR was considered with mode PID, for each time step, there appeared to be separation between GF and NGF storms. For instance, the mode PID in time step 1 (Fig. 10A) showed light rain as the dominant hydrometeor for both GF and NGF storms; however, the corresponding mean LDR values for that time (Fig. 8A) showed mean LDR values ≥ -25 dB for the GF storms compared to the NGF storms. This suggested that while the dominant hydrometeor was light rain for both GF/NGF storms, there was at least some mixed phase precipitation present in the GF storms relative to the NGF storms. Therefore, the dominate PID hydrometeor in conjunction with *A*LDR could be useful in differentiating GF and NGF storms.

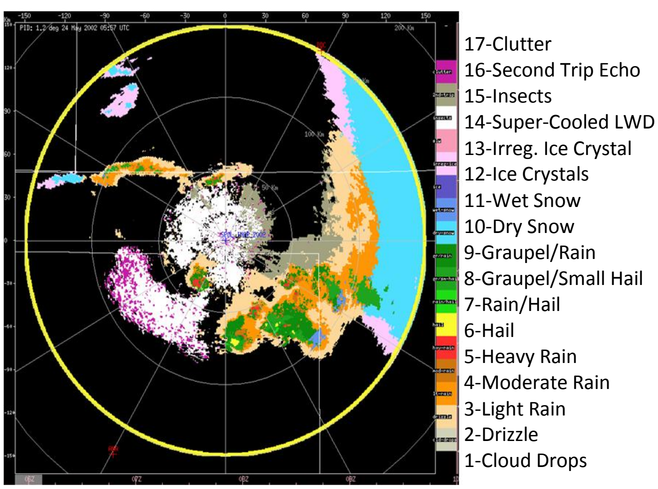

Figure 9. Example of the PID field displayed by S-Pol. The colors shown on the right-hand side correspond to PID numbers reserved for the hydrometeor types listed.

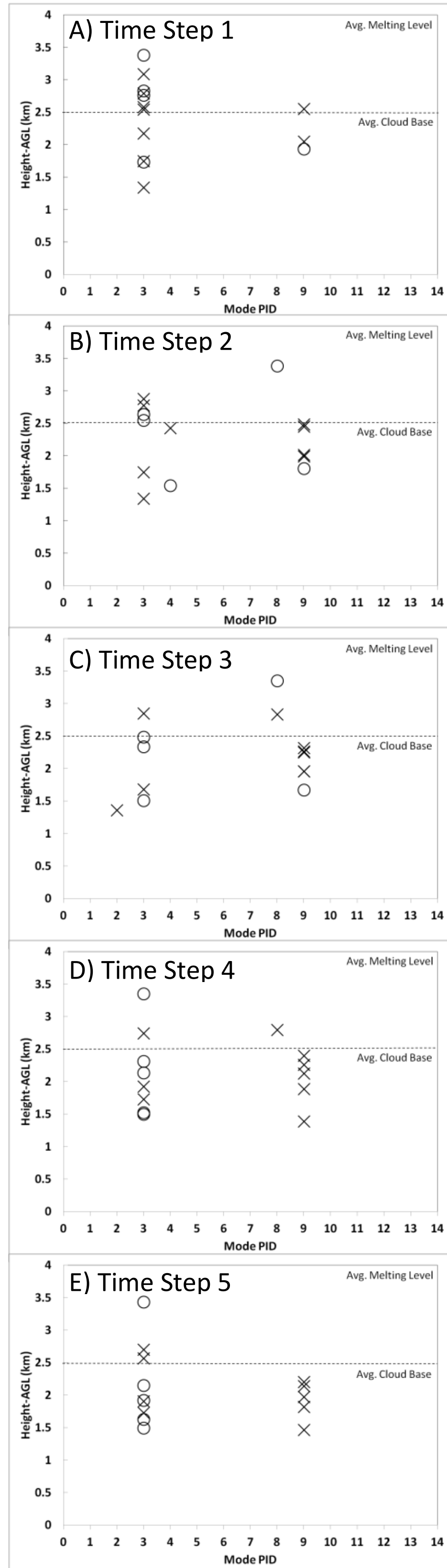

Figure 10. Mode PID for GF (X's) and NGF (O's) storms at A) time step 1, B) time step 2, C) time step 3, D) time step 4, and E) time step 5. The average melting and cloud base heights are also identified.

4.2 Environmental Conditions

Unlike the steps involved with storm characteristics, for environmental conditions running MRPP was straightforward since there was only "one time step" and 18 variables derived from the soundings to represent the pre-convective environment. As done with storm characteristics, all environmental conditions (rank values) were placed in MRPP to obtain a baseline p-value. Then, one-by-one each variable was removed and MRPP applied again to get a new p-value, which was used to calculate the delta p-value (baseline minus new). Again, if the delta p-value was negative, then the associated environmental variable was identified as significant, since removing the variable generated a worse p-value relative to the baseline p-value as shown in Table 5. MRPP was then applied once more but only on the environmental conditions found to be significant.

Table 5. MRPP results for environmental conditions. The (*) indicates the baseline p-value used for comparison. The conditions identified as significant were based on negative delta p-values (bold).

Environmental Conditions	P-Value	Delta P-Value
ALL*	0.302*	---
No Surface PT	0.301	0.001
No Surface VPT	**0.324**	**-0.022**
No Surface MR	0.284	0.018
No 700 mb MR	**0.328**	**-0.026**
No 400 mb T	0.289	0.013
No 400 mb PT	0.289	0.013
No 400 mb VT	0.287	0.015
No 400 mb VPT	0.287	0.015
No LCL	**0.344**	**-0.042**
No MLI	**0.327**	**-0.025**
No LFC	0.302	0.00
No Positive Area Below LFC	0.282	0.02
No Negative Area Above LFC	0.256	0.046
No CAPE	**0.313**	**-0.011**
No CIN	**0.321**	**-0.019**
No 0-6 km Shear	0.293	0.009
No Bulk Richardson Number	**0.341**	**-0.039**
No Melting Level	0.281	0.021

4.2.1 MRPP Results

From the 18 environmental conditions considered, MRPP results indicated that, with a p-value of 0.097, the **lifted condensation level**, **bulk Richardson number**, **700 mb mixing ratio**, **modified lifted index**, **surface virtual potential temperature**, **convective inhibition**, and **convective available potential energy** were *collectively* the most significant. Since each variable is a dimension, the separation/clustering of GF and NGF storms occurred in a 7 dimensional space, making it difficult to visualize. Instead, a simple statistical summary, utilizing actual values for the 7 environment variables, was incorporated (Table 6).

Based on mean values for the 7 environmental conditions, GF storms had higher CAPE (1023 vs. 554 J/kg), lower CIN (-224 vs. -384 J/kg), slightly higher surface VPT's (318 vs. 306 K), lower MLI's (-4 vs. -1), lower 700 MR's (3.9 vs. 5.0 g/kg), higher BRN's (27 vs. 9), and slightly higher LCL's (2.5 vs. 2.3 km) relative to NGF storms as shown in Fig. 11A-B.

Table 6. GF and NGF statistical storm summary for each of the 7 significant environmental conditions.

Environmental Conditions	GF Storms			NGF Storms		
	Min	Mean	Max	Min	Mean	Max
CAPE (J/kg)	11	1023	2494	11	555	2387
CIN (J/kg)	-520	-224	-66	-518	-384	-103
Surface VPT (K)	300	318	381	300	306	318
MLI	-7.80	-3.61	1.23	-7.01	-1.48	1.23
700 mb MR (g/kg)	2.50	4.0	6.0	2.80	5.10	6.50
BRN	0.30	27.0	67.0	0.30	9.20	36.4
LCL (mb, km)	681 (2.0)	753 (2.5)	812 (3.2)	718 (2.0)	790 (2.3)	812 (3.0)

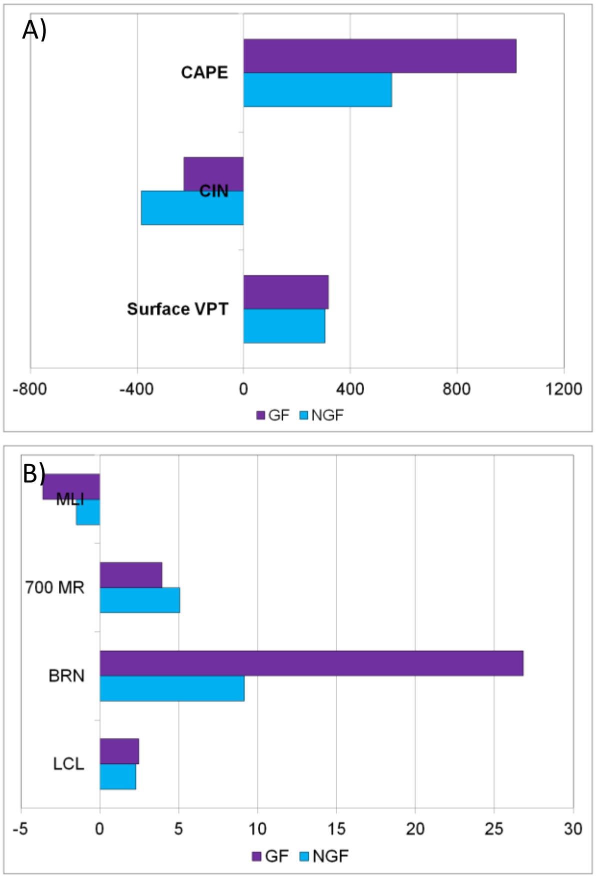

Figure 11. GF (purple) and NGF (blue) mean values for the 7 significant environmental conditions. CAPE (J/kg), CIN (J/kg), and surface VPT (K) are shown in A), while the MLI (unit less), 700 MR (k/kg), BRN (unit less), and LCL (km) are shown in B).

4.3 Interpretation

Based on the MRPP assessments for storm characteristics, it was surprising to observe the mean LDR as a strong candidate in discriminating GF and NGF storms. Interestingly enough, Vivekanandan et al. (1993) discussed that the presence of mixed-phase precipitation occurred with LDR signals ≥ -25 dB, which was found to be the exact threshold in differentiating GF and NGF storms for this study. Furthermore, unlike the other polarimetric variables, LDR is able to detect not only mixed-phase but also tumbling and irregular-shaped precipitation when it would require the use of reflectivity (Z), differential reflectivity (Zdr), and specific differential phase (Kdp) to do the same. And while Rho_{hv} is capable of detecting mixed-phase precipitation, it is unable to discriminate between hydrometeors such as light rain, snow, and graupel, which appeared to be important in this research.

Given that the depth/height of interest was between 1 and 4 km AGL, where 4 and 2.5 km were the average melting level and cloud base, respectively, it was suggested that the melting and evaporation processes of the dominant hydrometeors played a role in differentiating GF and NGF storms through time. The majority of GF storms transitioned from light rain to graupel-rain/graupel-small hail throughout the reflectivity core while the majority of NGF storms transitioned from light rain to moderate rain for roughly the same region. The hydrometeor, graupel, was observed more so in GF than NGF storms. In addition, it appeared that hydrometeor type, in conjunction with mean LDR, could be used to identify GF-producing thunderstorms. For instance, light rain and a high mean LDR (≥ -25 dB) is characteristic of GF storms, whereas light rain and low mean LDR (< -25 dB) is characteristic of NGF storms. All these indicators occurred some 10 to 40 min prior to when the gust fronts were detected on radar.

For environmental conditions, MRPP assessments on instability, moisture, and shear revealed there were 7 variables that differentiated GF and NGF storms. In terms of instability, GF storms had an unstable environment (mean MLI = -4) in which thunderstorms were likely to develop with some becoming severe as a result of a lifting mechanism(s). More specifically, the environment for GF storms favored stronger updrafts (higher mean CAPE) with moist buoyant air (slightly higher mean SVPT) and less negative buoyant air to overcome (lower mean CIN). For NGF storms, the environment was slightly unstable (mean MLI = -1) and needed the presence of a lifting mechanism for storms to develop, which in this study was most likely due to daytime heating. As mentioned earlier, the primary synoptic setup for NGF storms was the lack of large scale forcing combined with the fact that the region is strongly influenced by south/southeasterly flow and the low-level jet phenomenon, which can impede the formation and propagation of a gust front.

In terms of instability and shear, the GF storms had an environment that favored a balance between buoyancy and shear and in some cases the buoyancy dominated over the shear (higher mean BRN), which is characteristic of single and mulit-cell type thunderstorms. For NGF storms, shear dominated over the buoyancy, which is an environment not very conducive to thunderstorm and gust front development. Regarding moisture, it appeared that the environment was more favorable for GF storms when there was drier air aloft (lower mean 700 mb MR), which could be entrained into the storms further influencing the melting and evaporation processes on the hydrometeors. In addition, a higher mean cloud base (LCL), as observed in the GF storms, would suggest the precipitation had more time to cool the air appreciably through melting and evaporation resulting from the warm, dry air near the surface.

Based on the MRPP results, these selected storm characteristics and environmental conditions appeared to distinguish GF and NGF storms. With more research and more case studies, there is the potential to use these variables (and others) as criteria for GF forecasting.

5. Summary & Future Work

The purpose of this paper was to highlight the use of a rigorous statistical technique, MRPP, to differentiate GF and NGF thunderstorms observed during IHOP_2002. This research investigated the storm radar characteristics and environmental conditions of 14 single and multicell thunderstorms-9 GF and 5 NGF storms. S-Pol provided radar-observed storm characteristics, while soundings launched at three sites within S-Pol's domain (AMA, DDC, and ISS) provided environmental conditions. There were 7 radar-observed characteristics and 18 basic environmental conditions considered for MRPP.

To recap, MRPP examines the distances of data points within each group of interest and compares them to the distances of the data points between the different groups of interest using probability. Probability was used to test the null hypothesis that GF and NGF storms exhibited no differences in terms of radar storm characteristics and environmental conditions. More specifically, MRPP was used to determine which variables in radar storm characteristics and environmental conditions would tend to reject the null hypothesis. An MRPP test statistic, or p-value, of less than or equal to 0.1 (90% confidence level), was considered the significant threshold. For simplicity, radar storm characteristics and environmental conditions were analyzed separately.

For radar storm characteristics, MRPP was applied to each of the 5 time steps leading up to the divergence/decay time while, for the latter, MRPP was applied to the derived environmental variables. Once the significant variables were identified, they were then analyzed in depth to obtain specific information that could be used later in GF forecasting.

From the MRPP results on storm characteristics, the *A*LDR field appeared to differentiate GF and NGF storms some 40 min. prior to the divergence/decay times. More specially, a -25 dB threshold was identified around the average melting level and cloud base height (4 and 2.5 km, respectively) with GF storms having higher *A*LDR values relative to NGF storms. In addition, there were two predominant hydrometeor categories for the corresponding region: light rain and graupel/rain. GF storms saw a transition from light rain to graupel/rain that was not as apparent in the NGF storms. And when the dominant hydrometeor was considered with *A*LDR, they appeared to discriminate between GF and NGF storms. Therefore, given the region of interest (1-4 km AGL), most likely the melting and evaporation rates of graupel-rain cooled the air appreciably to produce the gust fronts observed in this study. However, whether the amount of graupel-rain present in a thunderstorm affects these rates and thus, gust front intensity, remains to be seen.

For environmental conditions, the MRPP analysis indicated that CAPE, CIN, surface VPT, MLI, 700 mb MR, BRN, and LCL differentiated GF and NGF storms. In general, GF storms had higher cloud base heights, higher instability, more wind shear, and lower moisture content aloft relative to NGF storms. The presence of higher instability and wind shear in GF storms indicated an environment more conducive for precipitation growth of various species and mixed-phase precipitation. Higher cloud base heights and lower mid-level moisture content inferred the entrainment of dry environmental air, which also likely contributed to the melting and evaporation rates of graupel-rain in GF storms.

However, this study was not without its challenges and limitations, particularly when extracting and setting the data up for MRPP. The main concerns are listed below:

- need for a larger sample of GF and NGF storms to determine if the significant storm and environmental variables found in this research are indeed generally significant,
- properly identifying GF and NGF storms given radar limitations, particularly with surface divergence identification and range dependency of storms,
- inconsistencies in the availability of radar measurements for different elevation angles (this prompted the data organization used in this study),
- properly thresholding radar fields (e.g., Z, Z_{dr}, K_{dp}),
- uncertainty with contouring time-height plots by hand and extracting data,
- location, timing, and availability of soundings (some soundings were used for both GF and NGF storms).

The following are suggestions for improvement:

- Full radar volume coverage and coverage of storms from initiation to dissipation; use higher temporal resolution of radar data,
- use of constant altitude plan position indicator radar data,
- use of modified soundings closer to the time storms initiated or modeled soundings to provide temporal environmental conditions,
- examine hydrometeor size distributions in depth,
- examine storm characteristics and environmental conditions together instead of separately,
- use a forward regression approach with MRPP instead of backwards regression to validate the results for both storm characteristics and environmental conditions, and
- incorporate other thunderstorm types, such as supercell thunderstorms and mesoscale convective systems.

Overall, there were specific storm and environmental variables that distinguished GF and NGF storms. While it is still too early to make any decisive remarks about the variables identified, this study does provide a foundation for future work with MRPP. For instance, MRPP could be used to identify all the factors that not only may forecast gust front storms but also influence gust front strength and propagation. This information could then be used in short-term forecasting, which currently has difficulty with developing and maintaining gust fronts. This information could also assist with forecasting tornadic thunderstorms, since the strength of its gust front can significantly influence tornadogenesis. As always, more research is needed.

Acknowledgements

The primary author would like to thank the following financial supporters of this research: the South Dakota School of Mines & Technology Atmospheric Science Department, the Significant Opportunities in Atmospheric Research and Science (SOARS) Program, and the National *Aeronautics and Space Administration (NASA)* South Dakota Space Grant Consortium. In addition the primary author would like to thank the following people for their time, effort, and guidance on various aspects of this research study: Tammy Weckwerth, Donna Kliche, Rita Roberts, Paul Smith, Mike Dixon, Scott Ellis, Jean Hurst, Greg Meymaris, Nancy Rehak, Jim Wilson, and Paul Mielke. Thank you!

References

Biondini M.E., P.W. Mielke, and K.J. Berry, 1988: Data-dependent permutation techniques for the analysis of ecological data. *Vegetatio.*, **75**, 161-168.

Gilmore, Matthew S., Jerry M. Straka, Erik N. Rasmussen, 2004: Precipitation and Evolution Sensitivity in Simulated Deep Convective Storms: Comparisons between Liquid-Only and Simple Ice and Liquid Phase Microphysics*. *Mon. Wea. Rev.*, **132**, 1897–1916.

Droegemeier, K. K., and R. B. Wilhelmson, 1987: Numerical simulation of thunderstorm outflow dynamics. Part I: Outflow sensitivity experiments and turbulence dynamics. *J. Atmos. Sci.,***44,** 1180–1210.

Goff R., 1976: Vertical Structure of Thunderstorm Outflows. *Mon. Wea. Rev.*, **104**, 1429–1440. Herzegh, P. H., 1988: Formulation of output parameters for PAM II CMF data. NCAR/FOF informal publication.

Hookings, G. A., 1965: Precipitation maintained downdrafts. *J. Appl. Meteorol.*, **4**, 190-195.

Johnson, R. H., and M. Nicholls, M. 1983: A compositive analysis of the boundary layer accompanying tropical squall line. *Mon. Weather Rev.*, **11**, 308-319.

Knight, Charles A., L. Jay Miller, Robert A. Rilling, 2008: Aspects of precipitation development in trade wind cumulus revealed by differential reflectivity at s band. *J. Atmos. Sci.*, **65**, 2563–2580.

McCaul, E. W., C. Cohen, 2002: The impact on simulated storm structure and intensity of variations in the mixed layer and moist layer depths. *Mon. Wea. Rev.*, **130**, 1722–1748.

McCune, B. and J.B. Grace, 2002: Chapter 24 – MRPP (Multi-response Permutation Procedures) and Related Techniques. In: McCune. B. and Grace, J.B. *Analysis of Ecological Communities*. pp. 188-197. *MJM Publishers*.

Mielke, P. W., K. J. Berry, and G. W. Brier, 1981: Application of multi-response permutation procedures for examining seasonal changes in monthly mean sea-level pressure patterns. *Mon. Wea. Rev.*, **109**, 120–126.

Rasmussen, R. M., V. Levizzani, H. R. Pruppacher, 1984: A wind tunnel and theoretical study on the melting behavior of atmospheric ice particles: III. experiment and theory for spherical ice particles of radius > 500 μm. *J. Atmos. Sci.*, **41**, 381–388.

Schlesinger, Robert E., 1999: Heat, Moisture, and Momentum Budgets of Isolated Deep Midlatitude and Tropical Convective Clouds as Diagnosed from Three-Dimensional Model Output. Part II: Sensitivity to Ice Phase and Small Changes in Ambient Shear Strength and Low-Level Moisture Supply. *J. Atmos. Sci.*, **56**, 3520–3543.

Simpson, J. E., 1969: A comparison between laboratory and atmospheric density currents. *Quart. J. Roy. Meteor. Soc*., **95**, 758-765.

Srivastava, R. C., 1987: A model of intense downdrafts driven by the Melting and Evaporation of Precipitation. *J. Atmos. Sci.*, **44**, 1752–1774.

Srivastava, R. C., 1988: On the Scaling of Equations Governing the Evolution of Raindrop Size Distributions. *J. Atmos. Sci.*, **45**, 1091–1092.

van den Heever, Susan C., William R. Cotton, 2004: The Impact of Hail Size on Simulated Supercell Storms. *J. Atmos. Sci.*, **61**, 1596–1609.

Vivekanandan, J., R. Raghavan, V. N. Bringi, 1993: Polarimetric radar modeling of mixtures of precipitation particles. *Geos. And Remot. Sens.,* **31**, 1017–1030.

Wakimoto, R. M., 1982: The life cycle of thunderstorm gust fronts as viewed with Doppler radar and rawinsonde data. *Mon. Wea. Rev.*, **110**, 1060-1082.

Weckwerth, Tammy M., David B. Parsons, 2006: A Review of Convection Initiation and Motivation for IHOP_2002. *Mon. Wea. Rev.*, **134**, 5–22.

Wilson, James W., Charles A. Knight, Sarah A. Tessendorf, Courtney Weeks, 2011: Polarimetric Radar Analysis of Raindrop Size Variability in Maritime and Continental Clouds. *J. Appl. Meteor. Climatol.*, **50**, 1970–1980.

Appendix A

To avoid contamination of bad data into the mean calculations, specific thresholds were applied to these radar fields.

Radar Field	Thresholds
Reflectivity	≥ 15 (dBZ)
Differential Reflectivity	-2 to 5 (dB)
Specific Differential Phase	-1 to 5 (deg km^{-1})
Copolar Correlation Coefficient	0.92 to 1.0
Linear Depolarization Ratio	-36 to -10
Particle Identification Field	1-14
Cross Polar Power	≥ -112 (dBm)